

NON-TRACKING-BASED 2D STRAIN ESTIMATION IN TAGGED MRI

Zhen Qian, Dimitris Metaxas

Rutgers University
Center for Computational Bio-Imaging and Modeling
Piscataway, NJ, 08854, USA

Leon Axel

New York University
Department of Radiology
New York, NY, 10016, USA

ABSTRACT

Tagged MRI is a non-invasive technique to assess myocardial deformations. In this paper, we developed a novel non-tracking-based strain estimation method for tagged MRI. This method is based on the extraction of tag's deformation gradient, and therefore avoids the limitations of conventional tracking-based strain estimators. We tested this method on both simulated and real world images. In simulated images, we quantitatively evaluated the accuracy and robustness of our non-tracking estimator. We find that the results of circumferential strain and local tissue rotation angle are highly consistent with the ground truth values. We also tested our method on both normal and patient data. Real world tests show our results are valuable to visually distinguishing normal and abnormal data, and have the potential to quantitatively diagnose cardiac malfunctions or diseases.

Index Terms— Tagged MRI, Strain analysis

1. INTRODUCTION

Cardiovascular diseases are the main cause of death in developed countries. Many cardiovascular diseases, such as ischemia and infarction, are associated with the alteration of the global or local contractility of myocardium. Accurately assessing the detailed myocardial deformation, such as the estimation of the local strain values, could be critical for the early diagnosis of cardiac diseases and dysfunctions.

Tagged cardiac magnetic resonance imaging (tMRI) [1] has been extensively used in clinical applications to non-invasively visualize the detailed myocardial deformation. The technique of tMRI generates sets of equally spaced parallel tagging lines within the myocardium as temporary material markers through spatial modulation of the magnetization. See Fig. 1 for some examples. The goal of this study is to quantitatively assess the myocardial strain values by extracting the deformation of the tag lines or grids.

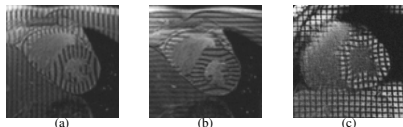


Fig. 1. Sample images of tMRI. (a) and (b) are from the same heart at the same imaging plane and have tagging lines that are perpendicular to each other. (c) has tagging grids. Our strain estimation method will work on both imaging settings.

In continuum kinematics, strain can be formulated as the derivative of displacement. Therefore, to estimate the myocardial strain from tMRI, many researchers have proposed tracking-based methods to first derive myocardial displacement. Then strain can be calculated from the displacement field. In [2], deformed tags are tracked and interpolated using a spline method to obtain the displacement map. Then the 2D Lagrangian strain is calculated from the horizontal and vertical displacement maps. In [3], 3D strain is derived from a 3D displacement map. A main difficulty of tag-tracking based methods is in balancing the internal and external forces of the deformable model that is used in the automated tracking process. If the internal forces are too small, then irregular tracking results, such as tag jumps, will present. If the internal forces are too big, then over-smoothed tags will lead to underestimated strain results. Another popular approach is using the HARP technique [4]. In [5, 6], myocardial velocity field and pathlines are calculated from the phase map using the HARP technique. Then strain is obtained from the HARP phase tracking results. A limitation of HARP-based methods is that they have difficulties in handling tags with large deformation. In addition, phase tracking is done by adding up the phase changes in each previous temporal frames. Therefore the tracking error is prone to accumulation.

In [7, 8], Gabor-filter-bank-based methods are proposed to extract tagging lines and myocardial deformation. Comparing with Fourier-transform-based methods, such as HARP, Gabor filter is a spatially localized method so that it is more adaptive to large tag deformation. In this paper, we propose a non-tracking 2D strain estimation method based on Gabor filter. At each pixel in the myocardium area, we extract the local tag distances and orientations in both x - and y - coordinates by searching for an optimal Gabor filter. Then the 2D strain and local rotation angle at each pixel can be obtained by using the strain formula in terms of deformation gradient. In this way, we don't need to track the tags or phase angles over time, and the limitations of tracking methods listed in the previous paragraph can be avoided. We first test our method on a series of phantom images and study the effectiveness of our Gabor-based strain estimation method. Then we apply this method on normal and patient data. From the experiments, we find that our strain estimation method is accurate and robust to noise. It has the potential to quantitatively diagnose cardiac malfunctions or diseases.

2. METHODOLOGY

2.1. Gabor Filter Design

2D Gabor filter is basically a 2D Gaussian multiplied by a complex 2D sinusoid [9]: $h(x, y) = g(x, y)s(x, y)$, where $g(x, y)$ is a 2D Gaussian, and $s(x, y)$ is a complex 2D sinusoid function: $s(x, y) = \exp[-j2\pi(Ux + Vy)]$.

In this application, we use a symmetric Gaussian envelope with $\sigma_x = \sigma_y = 1/\sqrt{U^2 + V^2}$, so that the rotation of the Gabor filter is determined only by the 2D frequencies of the complex sinusoid, which can be derived by $\phi = \arctan(V/U)$. The spacing between peaks of the sinusoid is determined by $S = 1/\sqrt{U^2 + V^2}$. A Gabor filter in our application can be defined with only two parameters U and V :

$$h(x, y) = \frac{U^2 + V^2}{2\pi} e^{-\left[\frac{(x^2+y^2)(U^2+V^2)}{2} + j2\pi(Ux+Vy)\right]} \quad (1)$$

A main advantage of Gabor filters is that they always achieve the minimum space-bandwidth product which is specified in the uncertainty principle due to their Gaussian envelopes [9]. At time 0 of the tagged MR imaging process, when the tagging lines or grids are initially straight and equally spaced with distance D , we set the initial parameters U_i and V_i of the Gabor filter to be equal to the frequencies of the image's first harmonic peaks in the spectral domain [7]. During a heart beat cycle, the tagging lines or grids deform with the underlying myocardium, and the spacing changes $m = S/D$ and orientation changes $\Delta\phi = \phi - \phi_i$ occur accordingly. We optimize U and V of the Gabor filter to fit the deformed local tag patterns, which means by convolving the optimal Gabor filter $h_o(U_o, V_o)$ with the local image patch I that centers at certain pixel (x, y) , we get the highest magnitude response. Then, we can extract the local deformations m and $\Delta\phi$.

$$(U_o, V_o) = \underset{U, V}{\operatorname{argmax}}(|h(U, V) * I|) \quad (2)$$

The optimization procedure can be performed using different strategies, such as gradient descent or simplex method. Since we only need to optimize two parameters U and V , in our experiment, the optimization converges very fast by using either method.

2.2. Strain Estimation

Instead of calculating the strain values in terms of the gradient of the displacement by tracking the tag pattern, we directly analyze the local tag deformation. For simplicity, we assume that the myocardium is incompressible, and it undergoes three possible deformations: stretching, compression, and local rotation. The initial tag spacings and orientations are referred to as the initial state, so that Lagrangian strains in beating myocardium can be obtained by comparing the deformed tags to the initial state.

For a myocardial element, we assume that in a certain coordinate system \mathbf{X} its initial length is $d\mathbf{X}$. After deformation, the myocardial element's length is $d\mathbf{x}$ in coordinate \mathbf{X} . At position \mathbf{x} we can define the deformation gradient

$\mathbf{F} = d\mathbf{x}/d\mathbf{X} = \nabla\mathbf{x}$ [10]. For 2D deformation gradient, as seen in Figure 2, the initial tag pattern has two sets of horizontal and vertical tagging lines with spacings equal to D_x and D_y . After myocardial deformation, the deformed tagging line spacings become S_x and S_y . The orientation changes of the tagging lines are $\Delta\phi_x$ and $\Delta\phi_y$. Then the deformation gradient tensor \mathbf{F} can be derived by:

$$\mathbf{F} = \begin{bmatrix} \frac{S_x \cos \Delta\phi_y}{D_x \sin \phi} & \frac{S_y \sin \Delta\phi_x}{D_x \sin \phi} \\ \frac{S_x \sin \Delta\phi_y}{D_y \sin \phi} & \frac{S_y \cos \Delta\phi_x}{D_y \sin \phi} \end{bmatrix} \quad (3)$$

where $\phi = \frac{\pi}{2} - \Delta\phi_x - \Delta\phi_y$. From the previous section, the spacing parameter m and orientation changes $\Delta\phi$ of the Gabor filter can be directly used to derive \mathbf{F} .

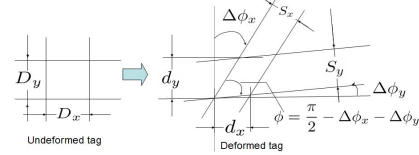


Fig. 2. The illustration of \mathbf{F} calculation. After tag deformation, $d_x = S_x \cos \Delta\phi_y / \sin \phi$, and $d_y = S_y \cos \Delta\phi_x / \sin \phi$, which are used in Equation. 3.

From \mathbf{F} , we can derive the Lagrangian finite strain tensor \mathbf{E} and local rotation matrix \mathbf{R} by:

$$\mathbf{E} = \frac{1}{2}(\mathbf{F}^T \cdot \mathbf{F} - \mathbf{I}) \quad (4)$$

$$\mathbf{R} = \mathbf{F}(\mathbf{F}^T \cdot \mathbf{F})^{-1/2} \quad (5)$$

where \mathbf{I} is an identity matrix.

2.3. Evaluation on Phantom Images

To evaluate our strain estimation method, we generate 5 frames of phantom images that simulate the contraction process of the left ventricular (LV) muscle. A main advantage of using phantom images is that our strain estimates can be easily compared with the ground truth. As seen in the first and second rows of Fig. 3, we generate a 2D LV phantom with both horizontal and vertical tagging lines in short axis, by adding 2D sinusoid patterns. Then the LV model undergoes incompressible deformation of contraction and rotation. At time t_4 , based on the calculation of the 2D area, the ejection fraction (EF) of this phantom is 75%, which is higher than human values in most cases, so that we guarantee this model can fit most clinical circumstances (In healthy heart, based on calculation of 3D volume, EF is about 55%–70% [11]. In diseased heart, this value tends to be smaller.)

In clinical tMRI imaging settings, the initial horizontal and vertical tag spacings are equal: $D_x = D_y = D$. Using Equation 2, the local deformations S_x/D , S_y/D , $\Delta\phi_x$ and $\Delta\phi_y$ can be obtained by optimizing the Gabor filter's frequency parameters U and V . In the third row of Fig. 3, the Gabor estimated local deformation maps at time t_4 are illustrated. For maps of S/D , the grey background equals 1, and brighter intensity corresponds to bigger tag spacing. For maps of $\Delta\phi$, the grey background equals 0, and brighter intensity stands for positive orientation change. We can find that our

Gabor filter optimization method achieves very smooth deformation maps that are consistent with the tag deformation patterns. Then the deformation gradient tensor \mathbf{F} , the strain tensor \mathbf{E} and the local rotation matrix \mathbf{R} can be derived from Equations 3, 4 and 5.

Other than the 2D horizontal-vertical Lagrangian strain tensor in Equation 4, in myocardial deformation research, we are more interested in the radial and circumferential strains. Positive and negative radial strains indicate myocardial thickening and thinning, respectively, while myocardial stretching and shortening are represented by positive and negative circumferential strains, respectively. We define an angle θ about the centroid of the LV, and transform \mathbf{E} into a radial-circumferential strain tensor $\hat{\mathbf{E}}$ with a rotation matrix $\mathbf{Q}(\theta)$, so that $\hat{\mathbf{E}} = \mathbf{Q}\mathbf{E}\mathbf{Q}^T$.

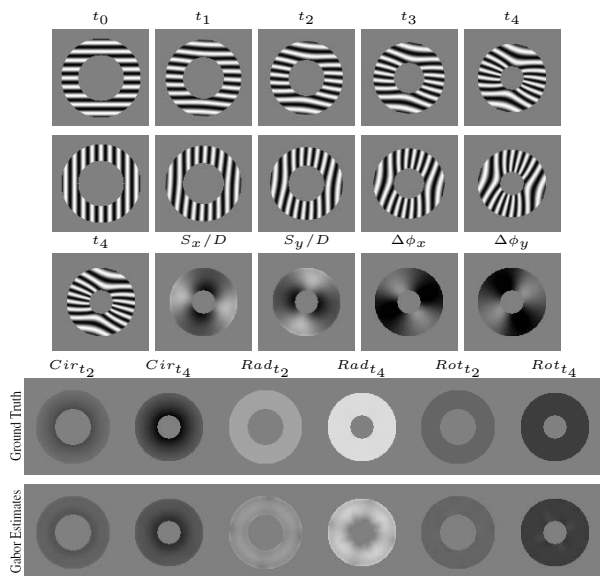


Fig. 3. The first and second rows are the simulated phantom images, which undergo an inward contraction with rotation from t_0 to t_4 . The third row is the deformations extracted from phantom images at t_4 using our Gabor filter method. The fourth and fifth rows are for comparison of ground truth and our estimation. Circumferential strain, radial strain and rotation angle at t_2 and t_4 are compared.

For quantitative evaluation, we calculate the means and standard deviations of the 2D strain and rotation angle. As seen in Fig. 4, we find that our method is most accurate in estimating rotation angle. For circumferential strain, our estimation matches with the ground truth well from t_1 to t_3 , and tends to underestimate when contraction gets bigger at t_4 (EF = 75%, which is rare in real human data). For radial strain, our method underestimates for every time frame, but still has the same trend as the ground truth.

Our non-tracking method calculates the local deformation at each single pixel. Therefore, in real data implementation, a major difficulty comes from the noisy nature of tMRI, which usually leads to irregular deformation maps. To solve this

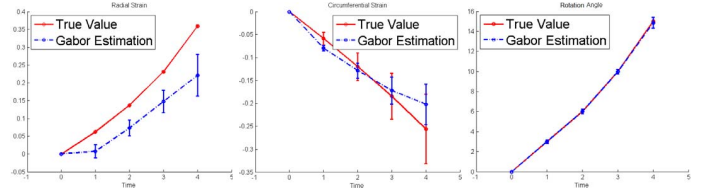


Fig. 4. Quantitative comparisons of the mean and standard deviation, at each time frame, of the radial strain (left-hand-side), the circumferential strain (middle) and the rotation angle (right-hand-side) show our estimations are consistent with the ground truth.

problem, we add a filtering loop to smooth out the noise. As illustrated in Fig. 6, in each iteration of the filtering loop, at each pixel, the local image patch is convolved with the estimated optimal Gabor filter. The convolution result is used to update the pixel's intensity, which is used in the next iteration. As seen in Fig. 5, the LV region LV_0 in the input image is noisy, thus without smoothing, the deformation maps S_{x_0}/D and $\Delta\phi_{x_0}$ are corrupted with error estimations. After 3 iterations of filtering the LV with the estimated Gabor filter at each pixel, the smoothed LV_3 gives more regular deformation maps S_{x_3}/D and $\Delta\phi_{x_3}$.

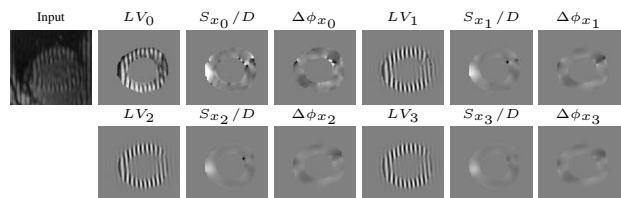


Fig. 5. A representative of real world tMRI whose LV region LV_0 is noisy, which leads to irregular estimations of S_{x_0}/D and $\Delta\phi_{x_0}$. After 3 smoothing iterations, we get a smoother LV_3 and better estimations of S_{x_3}/D and $\Delta\phi_{x_3}$.

However, smoothing the input image could be a dangerous strategy because it also smooths the myocardial deformations. Therefore we need to examine how smoothing loops affect the strain estimation. In the phantom images, at time t_4 , we apply filtering loops and observe how strain and rotation angle change. In Fig. 6, we see the estimations of rotation angle and circumferential strain do not change much after 4 smoothing loops. But radial strain estimation decreases after the first loop, and tends to be stable after a few iterations.

3. EXPERIMENTS ON REAL DATA

We tested our novel strain estimation method on both normal and patient data. For grid tagged MRI, we first separate the tag grids into 2 sets of tagging lines by a band-stop filter [12]. We estimate the strain and rotation angle only within the LV contours. To smooth out noise, we apply 3 iterations of the smoothing filter. In Fig. 7, we show a visual comparison of our estimates in a normal subject and a patient. For quantitative analysis, we divide the LV into 6 sectors, and calculate the means of strain and rotation angle in each sector at each time frame. In Fig. 8 we show the quantitative comparison.

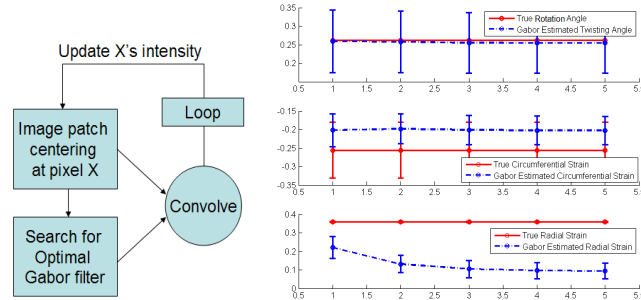


Fig. 6. Left hand side: The flowchart of the smoothing method. Right hand side: Quantitative analysis of the rotation angle (first row), the circumferential strain (second row) and the radial strain estimations (third row) w.r.t. the iteration number of the smoothing loop.

It is interesting to see that the magnitudes of the strain or rotation angle value are not the only criteria to diagnose abnormality. Their spatial and temporal distributions seem more important. Normal heart seems to have more smoothly distributed strain and rotation angle values. On the other hand, the patient heart seems to contract very hard at the 12 and 7 o'clock positions (indicated by the high strain magnitudes). However, most of the contraction is turned into a rotating motion (indicated by the big rotation angles), which makes the contractive efficiency poor. This suggests that the myocardial function should be assessed on comprehensive bases, including the strain magnitude, the regional strain pattern, and the regional tissue rotation pattern. Our novel strain estimation method works well in capturing the regional myocardial strain and rotation in tMRI.

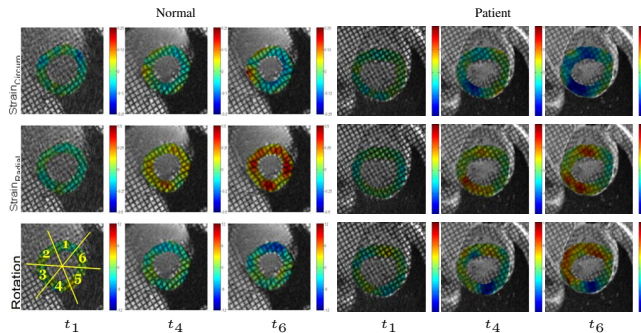


Fig. 7. Visual comparison of normal (left-hand-side) and patient's (right-hand-side) circumferential strain (first row), radial strain (second row) and rotation angle (third row) estimations at time t_1 , t_4 and t_6 . For quantitative analysis, we divide the LV into 6 sectors, which is illustrated in the lower-left image.

4. CONCLUSION AND FUTURE WORK

In this paper, we developed a novel non-tracking-based strain estimation method in tagged MRI. This method calculates strain by extracting the tag's deformation gradient, and avoids the limitations of conventional tracking-based strain estimators. We tested this method on both simulated and real world images. In simulated images, we quantitatively evaluate the accuracy and robustness of our non-tracking estimator. We

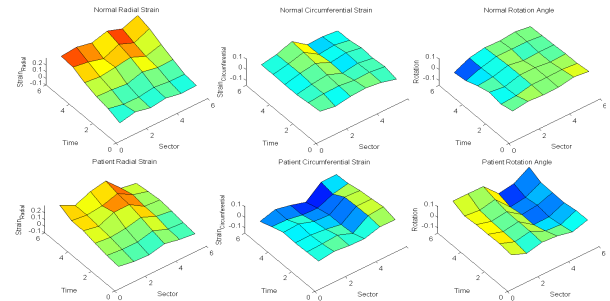


Fig. 8. In each LV sector, at each time frame, we calculate the mean value of the radial strain (left), the circumferential strain (middle) and the rotation angle (right) estimations. The colored surfaces illustrate the temporal and spatial distributions of the estimated values. The first row is from normal data. The second row is from patient data.

also tested our method on both normal and patient data. We find that our estimation results are highly consistent with simulated ground truth, and are potentially valuable to distinguishing the normal and abnormal data. In future work, we will develop the analysis of the strain and rotation patterns, in order to extract useful information to help with cardiac malfunction and disease diagnosis.

5. REFERENCES

- [1] L. Axel and L. Dougherty, "MR imaging of motion with spatial modulation of magnetization.," *Radiology*, vol. 171, pp. 841–845, 1989.
- [2] L. Axel, T. Chen, and T. Manglik, "Dense myocardium deformation estimation for 2D tagged MRI," in *FIMH*, 2005, pp. 446–456.
- [3] Douglas Bree et al, "Low-dose dobutamine tissue-tagged magnetic resonance imaging with 3-dimensional strain analysis allows assessment of myocardial viability in patients with ischemic cardiomyopathy," *Circulation*, vol. 114, pp. 133–136, 2007.
- [4] NF. Osman, WS. Kerwin, ER. McVeigh, and JL. Prince, "Cardiac motion tracking using CINE harmonic phase (HARP) magnetic resonance imaging," *Magnetic Resonance in Medicine*, vol. 42, pp. 1048–1060, 1999.
- [5] Nael F. Osman, Elliot R. McVeigh, and Jerry L. Prince, "Imaging heart motion using harmonic phase MRI," *IEEE Trans. Med. Imaging*, vol. 19, no. 3, pp. 186–202, 2000.
- [6] Nael F. Osman and Jerry L. Prince, "Visualizing myocardial function using HARP MRI," *Phys. Med. Biol.*, vol. 45, pp. 1665–1682, 2000.
- [7] Z. Qian, A. Montillo, D. Metaxas, and L. Axel, "Segmenting cardiac mri tagging lines using gabor filter banks," in *Proc of Int'l Conf. of the Engineering in Medicine and Biology Society*, 2003, pp. 630–633.
- [8] A. Montillo, L. Axel, and D. Metaxas, "Extracting tissue deformation using gabor filter banks," in *Proc of SPIE: Medical Imaging: Physiology, Function, and Structure from Medical Images*, 2004, vol. 5369, pp. 1–9.
- [9] D. Dunn, W. E. Higgins, and J. Wakeley, "Texture segmentation using 2-d gabor elementary functions," *IEEE Trans. Pattern Anal. and Machine Intell.*, vol. 16, pp. 130–149, 1994.
- [10] W. M. Lai, *Introduction to Continuum Mechanics*, Butterworth-Heinemann, 3rd edition, 1993.
- [11] Pfisterer M. E., Batter A., and Zaret B. L., "Range of normal values for left and right ventricular ejection fraction at rest and during exercise assessed by radionuclide angiography," *European Heart Journal*, vol. 6, no. 8, 1985.
- [12] Z. Qian, R. Huang, D. Metaxas, and L. Axel, "A novel tag removal technique for tagged cardiac MRI and its applications," in *Proc. of IEEE Int'l Symposium on Biomedical Imaging*, 2007, pp. 364–367.